Applied Mathematics 2013, 3(1): 1-11
DOI: 10.5923/j.am.20130301.01

Comparing up and Down Milling Modes of End-Milling Using Temporal Finite Element Analysis

Chigbogu G. Ozoegwu*, Sam N. Omenyi, Sunday M. Ofochebe, Chinonso H. Achebe

Department of Mechanical Engineering, Nnamdi Azikiwe University Awka, PMB 5025 Anambra state, Nigeria

Abstract Two types of end milling at partial radial immersion are distinguished in this work, namely; up and down end-milling. They are theoretically given comparative study for a three tooth end miller operating at 0.5, 0.75 and 0.8 radial immersions. 0.5 and 0.8 radial immersion conditions are chosen so that analysis covers situations in which repeat and continuous tool engagements occur while 0.75 radial immersion just precludes tool free flight. It results from analysis that the down end-milling mode is better favoured for workshop application than the up end-milling mode from both standpoints of cutting force and chatter stability. This superiority in chatter stability is quantified by making use of the Simpson's rule to establish that switching from up end-milling mode to down end-milling mode at 0.5 radial immersion almost doubles the possibility of chatter free milling while at 0.75 and 0.8 radial immersions this possibility almost triples. This result conforms to the age long recognition from workshop practices that climb milling operations are much more stable than conventional milling operations. Validation of the resulting stability charts is conducted via MATLAB dde23 time domain numerical analysis of selected points on the parameter plane of spindle speed and depth of cut.

Keywords Up end-milling, Down End-milling, Temporal Finite Elements, Phase Trajectories, Simpson's Rule

1. Introduction

Machining is needed for the production of specialized components in the aerospace, marine, automobile and other industries. For this reason best mode of machining is sought after for best productivity and quality of components. Among other methods of machining, end milling is extensively used in the industry. In end milling a machined surface that is at right angle with the cutter axis results as shown Figure 1. Milling cutters equipped with shanks for mounting on the spindle are utilized for end milling.

Two types of end-milling at partial radial immersion are distinguished as shown in figure 2. Milling operation as depicted in figure 2.a dynamically looks like the conventional milling since workpiece feed is in opposite direction to cutter rotation at advent of tooth-workpiece engagement. Chip thickness progressively grows from zero to non-zero values as feed progresses in this type of milling. The end milling process of figure 2.b dynamically resembles the climb milling being that workpiece feed is in the same direction as cutter rotation at inception of a tooth-workpiece engagement. Chip thickness starts from non-zero value and ends at zero value in this type of milling. These milling processes will thus be referred to in this work as up end-milling and down end-milling respectively. Radial immersion ρ is defined for these milling processes to mean the ratio of the radial depth of cut to the tool diameter. The aim here is to compare the cutting forces and stability of both types of end milling process for a three tooth milling tool at half, three-quarters and four-fifths radial immersions.

The first major difference between this work and others is that the cutting force of the non-chattered down end-milling and up end-milling are compared. It is suggested that there is less possibility of fatigue in the down end-milling mode since its magnitude of unperturbed cutting force is always less than that of the up end-milling at all radial immersions.

The superiority of conventional milling over climb milling in terms of surface quality of component in workshop practice is long known and documented[1-3]. It is noted by Joshi[2] that conventional milling has fixture or clamping problems that is entirely absent in climb milling. This is due to the lift effect cutting forces have on the workpiece in conventional milling. Miller and Miller[3] wrote that climb milling allows faster material removal rate and surface finish than conventional milling. The poorer surface finish in conventional milling is attributed to tooth-workpiece rubbing that occurs before active engagement. The fixture and rubbing-induced surface problem of conventional milling are not expected in up end-milling since the machined surface is at right angle with the cutter axis.

The dynamic resemblance of up and down end-milling with conventional and climb milling respectively is considered to mean resemblance in stability. Analysis shows that domain of chatter stability of down milling mode is much greater than that of up milling mode at all the studied

* Corresponding author:
chigbogug@yahoo.com (Chigbogu G. Ozoegwu)
Published online at http://journal.sapub.org/am

radial immersion conditions. The point thus made in this work is that the superiority of surface finish in climb milling over that in conventional milling is partly due to less possibility of chatter or unstable self –excited vibrations in the former. This is another contribution of this work.

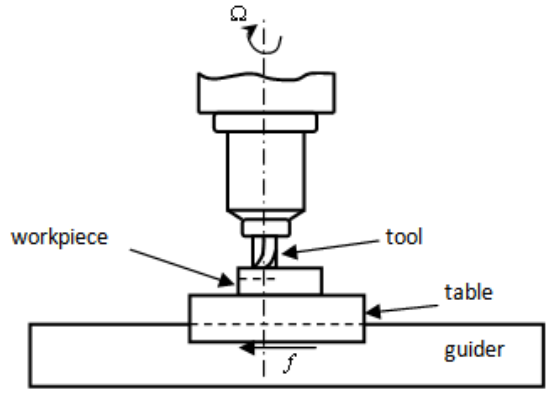

Figure 1. End-Milling

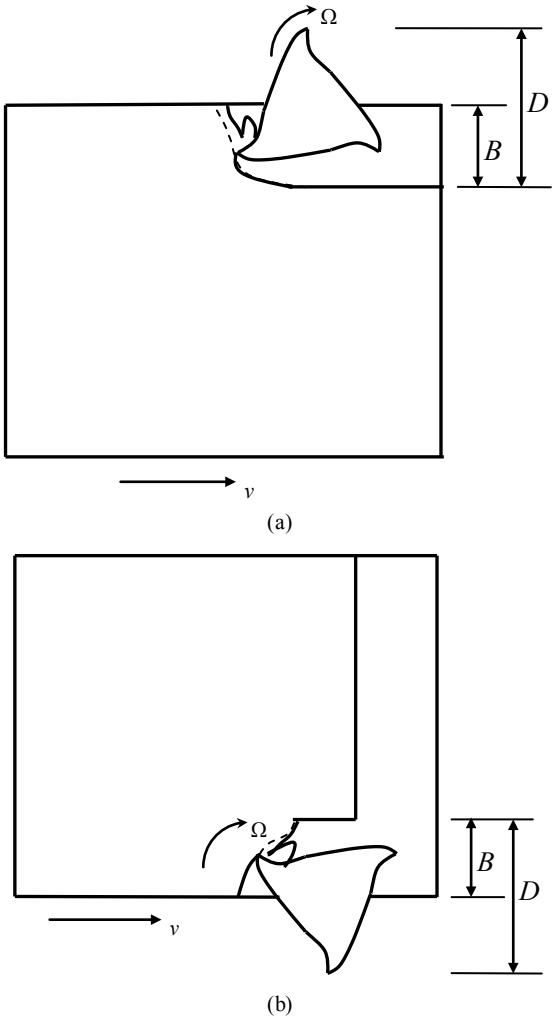

Figure 2. Two End-Milling Modes. (A) Up End-Milling; (B) Down End-Milling

The novelty of this work also lies in the use of Simpson's rule to quantify the superiority of chatter stability of down end-milling over up end-milling at each of the radial immersion conditions considered. It is found that switching from up end-milling mode to down end-milling mode at 0.5 radial immersion almost doubles the possibility of chatter free milling in the spindle speed range $0 < \Omega \leq 30000$ while at 0.75 and 0.8 radial immersions this possibility almost triples in the same spindle speed range.

2. Mathematical Model of Periodic Cutting Force

End-milling process as depicted in figure 3 is a multi-toothed cutting operation. The tool is given a spindle speed Ω in revolutions per minute while the workpiece has a prescribed feed velocity v imparted on it via the worktable.

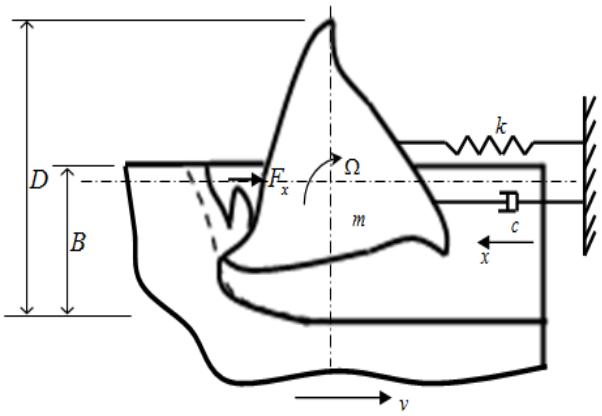

Figure 3. Dynamical Model Of End-Milling

A tool-workpiece disposition as shown in figure 4 is considered for the jth tooth of the tool where the normal and tangential components are designated $F_{norm\ ,j}(t)$ and $F_{tan\ ,j}(t)$ respectively. The x –component of cutting force for the tool thus becomes

$$F_x(t) = \sum_{j=1}^{N} g_j(t)\left[F_{norm\ ,j}(t)\sin\theta_j(t) + F_{tang\ ,j}(t)\cos\theta_j(t)\right] \quad (1)$$

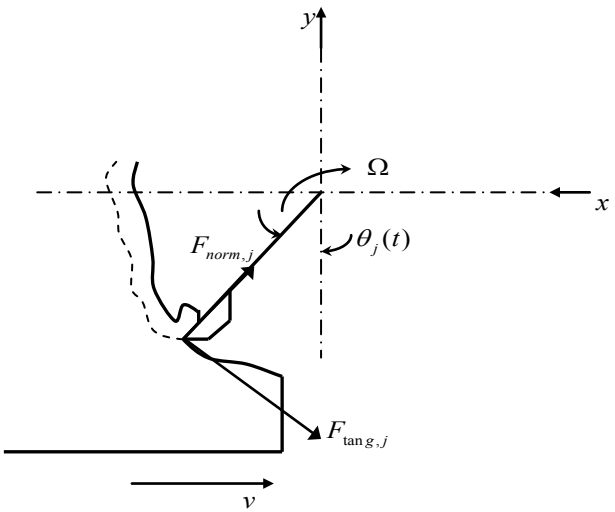

Figure 4. Milling Tooth-Workpiece Disposition

N is the number teeth on the milling tool indexed with the values $j = 1, 2, 3.....N$. The instantaneous angular position of a tooth j is $\theta_j(t)$. In this work $\theta_j(t)$ is measured clockwise relative to the negative $y-$axis to give

$$\theta_j(t) = \left(\frac{\pi\Omega}{30}\right)t + (j-1)\frac{2\pi}{N} + \alpha \tag{2}$$

where α is the initial angular position of the tooth indexed1. Screen or switching function for the jth tooth $g_j(t)$ could either have the values 1 or 0 depending on whether the tooth is active or not. For given start and end angles of cut designated θ_s and θ_e respectively, $g_j(t)$ of the general tool-workpiece disposition shown in figure 5 becomes[4]

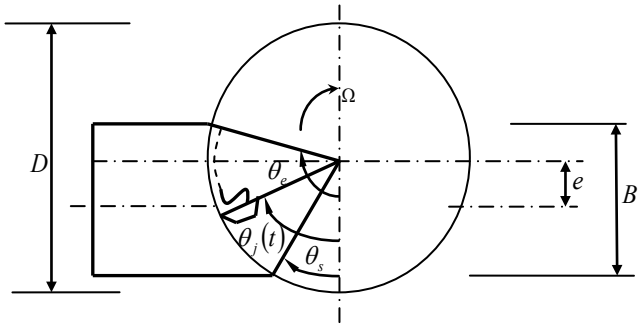

Figure 5. General Milling Tool-Workpiece Disposition

$$g_j(t) = \frac{1}{2}\left(1 + sgn\left\{sin\left[\theta_j(t) - arctan\left(\frac{sin\,\theta_s - sin\,\theta_e}{cos\,\theta_s - cos\,\theta_e}\right)\right] - sin\left[\theta_s - arctan\left(\frac{sin\,\theta_s - sin\,\theta_e}{cos\,\theta_s - cos\,\theta_e}\right)\right]\right\}\right) \tag{3}$$

where it is seen from figure 5 that

$$\begin{aligned}\cos\theta_s &= \frac{B+2e}{D}\\ \cos\theta_e &= \frac{2e-B}{D}\end{aligned} \tag{4}$$

B is the radial dept of cut, D is the tool diameter and e is the deviation of centre of radial dept of cut from the tool centre. For the studied end-milling tool-workpiece disposition shown in figure 2 the radial immersion ρ by definition becomes

$$\rho = \frac{B}{D} \tag{5}$$

Equation (5) put into equation (4) gives

$$\begin{aligned}\cos\theta_s &= \rho + \frac{2e}{D}\\ \cos\theta_e &= -\rho + \frac{2e}{D}\end{aligned} \tag{6}$$

If the radial immersion is given as $\rho = 1/d$, it will not be difficult to see from figure 2 that the deviation e is given as

$$e = \begin{cases}(d-1)\frac{D}{2d} & \text{for up end} - \text{milling}\\ (1-d)\frac{D}{2d} & \text{for down end} - \text{milling}\end{cases} \tag{7}$$

Equation (7) and (6) put into (3) while recalling that $\rho = 1/d$ gives the screen function in terms of radial immersion ρ for up end-milling as

$$g_j(t) = \frac{1}{2}\left\{1 + \text{sgn}\left[\sin\left(\theta_j(t) - \arctan\left\{\frac{-1}{2\rho}\sin[\arccos(1-2\rho)]\right\}\right) + \sin\left(\arctan\left\{\frac{-1}{2\rho}\sin[\arccos(1-2\rho)]\right\}\right)\right]\right\} \tag{8}$$

while for down end-milling the screen function in terms of radial immersion ρ becomes

$$g_j(t) = \frac{1}{2}\left\{1 + sgn\left[\sin\begin{matrix}\left(\theta_j(t) - arctan\left\{\frac{1}{2\rho}\sin[arccos(2\rho-1)]\right\}\right)\\ -\sin\left(arccos(2\rho-1) - arctan\left\{\frac{1}{2\rho}\sin[arccos(1-2\rho)]\right\}\right)\end{matrix}\right]\right\} \tag{9}$$

It is seen from figure2 that an N-tooth end miller could undergo free flight or damped natural vibration when the radial immersion gets too low. The condition for this to occur becomes

$$\theta_e - \theta_s < \frac{2\pi}{N} \tag{10}$$

Up end-milling as shown in figure 2 has start and end angles expressed from equations (6) and (7) in terms of radial immersion ρ as $\theta_s = 0$ and $\theta_e = \arccos(1-2\rho)$ while for down end-milling $\theta_s = \arccos(2\rho-1)$ and $\theta_e = \pi$. If these angles are put into the inequality (10), the restriction on radial immersion ρ for damped natural vibration for both Up end-milling and down end-milling becomes

$$\rho < \frac{1}{2}\left\{1 - \cos\left(\frac{2\pi}{N}\right)\right\} \tag{11}$$

The time spent in free flight t_f evidently becomes given as $t_f = \frac{30}{\pi\Omega}\left\{\frac{2\pi}{N} - (\theta_e - \theta_s)\right\}$. The ratio of time interval of free flight to discrete delay becomes $r_t = \frac{t_f}{\tau} = 1 - \frac{N}{2\pi}(\theta_e - \theta_s)$. If the start and end angles are put into this expression for r_t, the equations describing r_t for Up end-milling and down end-milling respectively becomes equations (12) and (13)

$$r_t = 1 - \frac{N}{2\pi}\arccos(1-2\rho) \tag{12}$$

$$r_t = 1 - \frac{N}{2\pi}[\pi - \arccos(2\rho-1)] \tag{13}$$

Total x-component of cutting force for the tool becomes given as

$$F_x(t) = \sum_{j=1}^{N} g_j(t)\left[F_{norm\,,j}(t)\sin\theta_j(t) + F_{tang\,,j}(t)\cos\theta_j(t)\right] \quad (14)$$

The tangential cutting force for the j tooth $F_{tang\,,j}(t)$ as indicated in figure 4 is given by the non-linear law[4]

$$F_{tang\,,j}(t) = Cw\left[f_a \sin\theta_j(t)\right]^{\gamma} \quad (15)$$

where w is depth of cut, C is the cutting coefficient associated with the workpiece material, f_a is the actual feed and γ is an exponent that is not greater than one, having a value of $3/4$ for the three-quarter rule. The empirical relationship connecting the milling tangential and normal cutting forces shown in figure 4 is written in[4] to be seen in the works of Balint, Bali and Tlusty to have the form

$$F_{norm\,,j}(t) = 0.3F_{tang\,,j}(t) \quad (16)$$

The actual feed rate f_a is the difference between present and one period delayed position of tool, thus

$$f_a = x(t) - x(t-\tau) \quad (17)$$

Equations (15), (16) and (17) are taken together to give

$$F_x(t) = wq(t)\left[x(t) - x(t-\tau)\right]^{\gamma} \quad (18)$$

where $q(t) = \sum_{j=1}^{N} g_j(t) C \sin^{\gamma}\theta_j(t)\left[0.3\sin\theta_j(t) + \cos\theta_j(t)\right]$ is a $\tau(=\frac{60}{N\Omega})$ periodic function since tool-workpiece disposition repeats after every time $t = \tau$ interval.

Stationary milling is the needed ideal that can only occur when there are no perturbations. In stationary milling the actual feed $f_a = x(t) - x(t-\tau)$ becomes equal to the prescribed feed per cutting period. That is, $f = v\tau$ such that equation (18) becomes

$$F_x(t) = (v\tau)^{\gamma} wq(t) \quad (19)$$

This is the periodic cutting force about which the realistic cutting force of equation (18) varies. If the milling process is stable, an initially chaotic cutting force will tend to equilibrium periodic cutting force as initial vibration dies out. The cutting force of stationary milling as given in equation (19) is τ-periodic like $q(t)$. For a milling process with the typical specification[5]; $C = 3.5 \times 10^7\,\mathrm{Nm}^{-7/4}$, $\gamma = 0.75$ (from the three-quarter rule), feed speed $v = 0.0025\mathrm{m/s}$, $\Omega = 2000$ rpm and $w = 0.001\mathrm{m}$, a plot of periodic cutting force over interval of two periods is produced for both up end-milling and down end-milling at 0.5, 0.75 and 0.8 radial immersions as shown in figure6a, b and c respectively. It is seen that at each radial immersion $F_x(t)$ has two different amplitudes, one above and other below the line $F_x(t) = 0$. The bigger amplitude of each periodic cutting force about zero value is of interest. The bigger the amplitude, the more likely the machined component will have tolerance error. At 0.5 radial immersion the cutting force amplitudes are 4.4 N and -2.7 N while they are 4.4 and 4.05 at 0.75 radial immersion for up end-milling and down end-milling respectively. Negative sign is retained to capture the meaning that cutting force is opposite to feed. At 0.8 radial immersion the cutting force amplitudes are 4.5 N and 4.15 N for up end-milling and down end-milling respectively. A plot of amplitude variation with ρ is given in figure 7 in which is seen that up end-milling has higher amplitude than the down end-milling in the entire range of radial immersion. The conclusion drawn becomes that Though the Taylors's tool life equation suggests equal longevity for up end-miller and down end-miller, the former is more damaging to tool than the latter since it generally has higher periodic cutting force amplitude. Reversal in direction of cutting force over a period exists for the down end-miller at low radial immersions since it has both positive and negative values when $\rho < 0.5$. This means that its vibratory motion occurs on both sides of the tool's undisplaced equilibrium position. This is not the case for the up end-miller. It is seen that when $\rho > 0.5$, amplitude of stationary cutting force of interest for down end-milling becomes positive and approaches that of up end-milling as ρ increases. It should be observed that cutting force varnishes over a time interval that is equal for both up end-milling and down end-milling. During this time interval which is given as $t_f = \frac{30}{\pi\Omega}\left[\frac{2\pi}{N} - \arccos(1-2\rho)\right]$ for up end-milling and $t_f = \frac{30}{\pi\Omega}\left[\frac{2\pi}{N} - \pi + \arccos(2\rho - 1)\right]$ for down end-milling, the tool is not engaged with the workpiece thus in transient response.

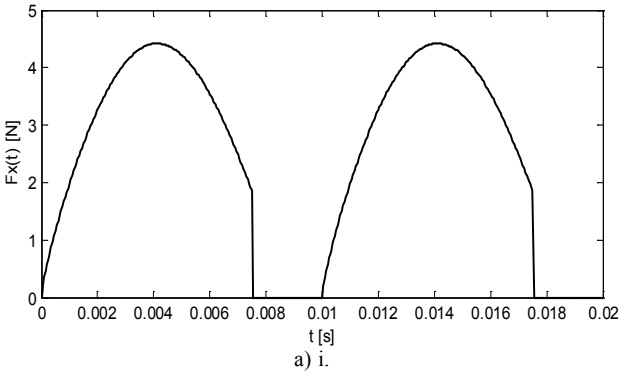

a) i.

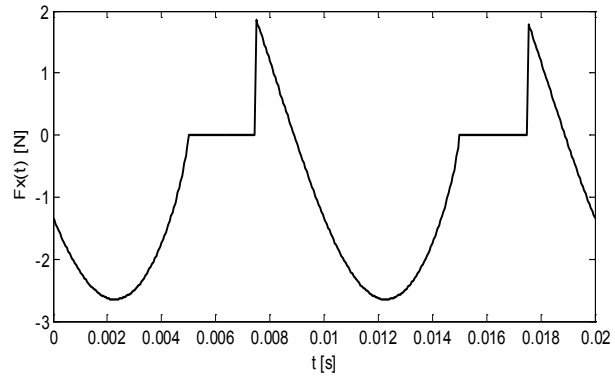

a) ii.

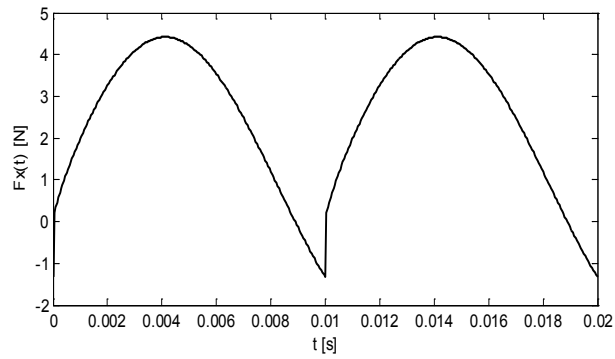

b) i.

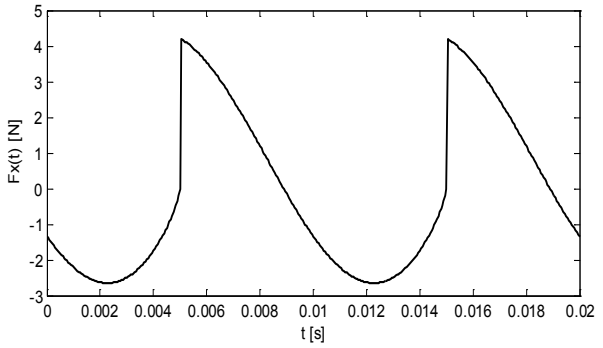

b) ii.

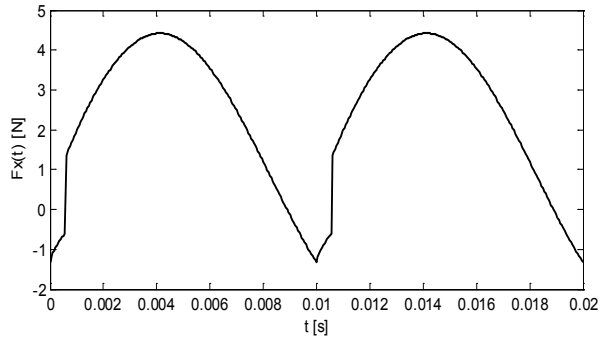

c) i.

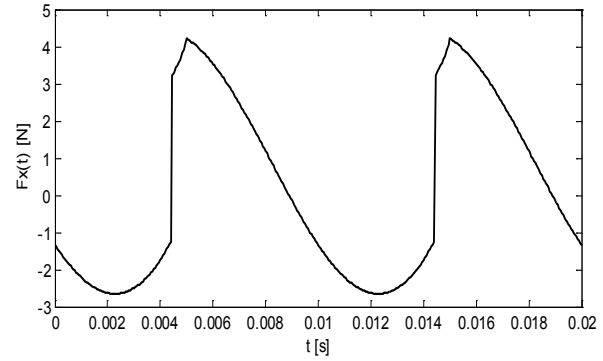

c) ii.

Figure 6. Stationary Cutting Force Variation for a Three Tooth End-Milling At (A) $\boldsymbol{\rho = 0.5}$, (B) $\boldsymbol{\rho = 0.75}$ and (C) $\boldsymbol{\rho = 0.8}$: I. Up End-Milling, Ii. Down End-Milling

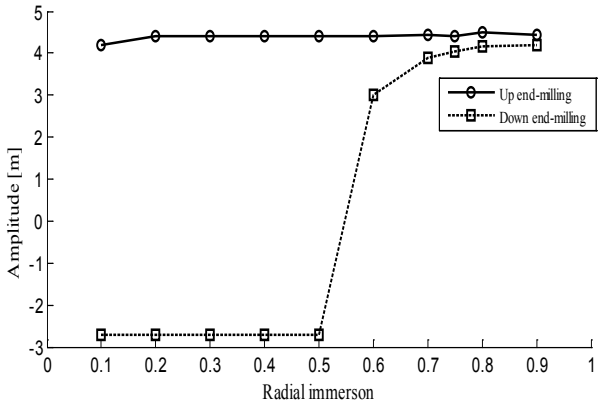

Figure 7. Amplitude of Stationary Cutting Force Variation Plotted Against Radial Immersion. Up End-Milling is Seen to Have Amplitude That is Fairly Invariant at about 4.4 N with $\boldsymbol{\rho}$ While Down End-Milling is Fairly Invariant At About -2.7 N Up To $\boldsymbol{\rho = 0.5}$

3. Equation of Regenerative Vibration

The parameters of the milling process as depicted on the dynamical model of figure 3 are; m mass of tool, c the equivalent viscous damping coefficient of the tool system and k the stiffness of the tool system. These modal parameters could be extracted from plot of the tool frequency response function in a scheme of experimental modal analysis[6-8]. Figure 3 is a single degree of freedom vibration model of an end milling tool. Most encountered resonance in machining involves the fundamental natural frequency thus single degree of freedom vibration is satisfactory when it is well separated from the higher natural frequencies as seen in Stepan[9]. *Chatter* is an unstable vibration in machining due regenerative effects that are originally triggered by internal and external perturbations. Regenerative effect as seen in figure 3 is the effect of waviness created on a machined surface due to perturbed dynamic interaction between the tool and the workpiece. The present tool pass that is indicated as dashed curve has waviness that is not in phase with the last tool profile. A variation in chip thickness causes cutting force variation that results in vibration which subsequently builds up to chatter if cutting parameter combination is unfavourable.

The free-body diagram for the tool dynamics shown in figure 3 is as depicted in figure 8.

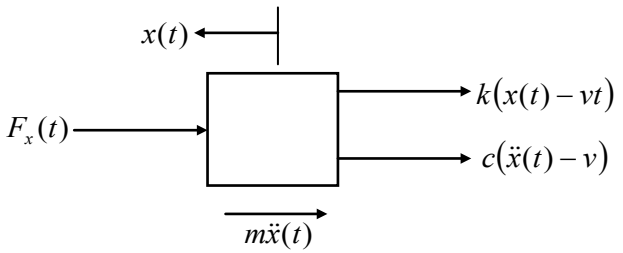

Figure 8. Free-Body Diagram Of Tool Dynamics

The differential equation governing the motion of the tool as seen from the free-body diagram is

$$m\ddot{x}(t) + c[\dot{x}(t) - vt] + k[x(t) - vt] + F_x = 0 \quad (20)$$

Introducing Equation (18) into the equation (20) gives

$$m\ddot{x}(t) + c[\dot{x}(t) - vt] + k[x(t) - vt] + wq(t)[x(t) - x(t-\tau)]^{\gamma} = 0 \quad (21)$$

The motion of the tool is assumed to be a linear superposition of prescribed feed motion vt, tool τ-periodic response $x_t(t)$ due to periodic force of equation (19) and perturbation $z(t)$[4] then

$$x(t) = vt + x_t(t) + z(t) \quad (22)$$

Substitution of equation (22) into equation (21) gives

$$m\ddot{x}_t(t) + c\dot{x}_t(t) + kx_t(t) + m\ddot{z}(t) + cz\dot{(t)} + kz(t) = -wq(t)\{v\tau + [z(t) - z(t-\tau)]\}^{\gamma} \quad (23)$$

Without perturbation (that is $z = z(t-\tau) = 0$), equation (23) simplifies to

$$m\ddot{x}_t(t) + c\dot{x}_t(t) + kx_t(t) = -wq(t)(v\tau)^{\gamma} \quad (24)$$

This governs the periodic motion of the system. Equation (24) means that equation (23) becomes

$$m\ddot{z}(t) + cz\dot{(t)} + kz(t) = wq(t)(v\tau)^{\gamma} - wq(t)\{v\tau + [z(t) - z(t-\tau)]\}^{\gamma} \quad (25)$$

Linearized Taylor series of equation (25) about $v\tau$ becomes

$$m\ddot{z}(t) + c\dot{z}(t) + kz(t) = -wh(t)[z(t) - z(t-\tau)] \quad (26)$$

where $h(t) = \gamma(v\tau)^{\gamma-1}q(t)$ is the τ-periodic specific force variation. Equation (26) is re-written with the following compact notations; $z(t) = z$ and $z(t-\tau) = z_\tau$ to give the periodic damped delayed differential equation of regenerative vibration of the system

$$\ddot{z} + 2\xi\omega_n\dot{z} + \left(\omega_n^2 + \frac{wh(t)}{m}\right)z = \frac{wh(t)}{m}z_\tau \quad (27)$$

With the substitutions $y_1 = z$ and $y_2 = \dot{z}$ made, equation (27) could be put in state differential equation form as

$$\begin{Bmatrix}\dot{y}_1\\ \dot{y}_2\end{Bmatrix} = \begin{bmatrix}0 & 1\\ -\left(\omega_n^2 + \frac{wh(t)}{m}\right) & -2\xi\omega_n\end{bmatrix}\begin{Bmatrix}y_1\\ y_2\end{Bmatrix} + \begin{bmatrix}0 & 0\\ \frac{wh(t)}{m} & 0\end{bmatrix}\begin{Bmatrix}y_{1,\tau}\\ y_{2,\tau}\end{Bmatrix} \quad (28)$$

Where $y_{i,\tau} = y_i(t-\tau)$ for $i = 1$ and 2. The natural frequency and damping ratio of the tool system are given in terms of modal parameters k, m and c respectively as $\omega_n = \sqrt{k/m}$ and $\xi = c/2\sqrt{mk}$. These modal parameters are easily extracted from experimental plot of the tool frequency response function $R(\omega) = X/F = 1/\sqrt{(k-\omega^2 m)^2 + \omega^2 c^2}$ for forced single degree of freedom vibration. The damped natural vibration that occurs during the time interval $t_f = \frac{30}{\pi\Omega}\left\{\frac{2\pi}{N} - \theta e - \theta s\right.$ obeys the ordinary differential equation

$$\ddot{z} + 2\xi\omega_n\dot{z} + \omega_n^2 z = 0 \quad (29)$$

since $h(t) = 0$. Putting the solution of form $z(t) = Ke^{\lambda t}$ into equation (29) the characteristic equation becomes

$$\lambda^2 + 2\xi\omega_n\lambda + \omega_n^2 = 0 \quad (30)$$

With the roots $\lambda_{1,2} = -\omega_n\xi \pm \omega_n\sqrt{\xi^2 - 1}$ such that the transient response becomes

$$z(t) = K_1 e^{\lambda_1 t} + K_2 e^{\lambda_2 t} \quad (31)$$

Assuming the initial conditions $z(0)$ and $\dot{z}(0)$, the constants become $K_1 = \frac{\dot{z}(0) - \lambda_2 z(0)}{\lambda_1 - \lambda_2}$ and $K_1 = \frac{\lambda_1 z(0) - \dot{z}(0)}{\lambda_1 - \lambda_2}$ resulting in the response vector becoming

$$\begin{Bmatrix}y_1(t)\\ y_2(t)\end{Bmatrix} = \frac{1}{\lambda_1 - \lambda_2}\begin{bmatrix}\lambda_1 e^{\lambda_2 t} - \lambda_2 e^{\lambda_1 t} & e^{\lambda_1 t} - e^{\lambda_2 t}\\ \lambda_1\lambda_2 e^{\lambda_2 t} - \lambda_1\lambda_2 e^{\lambda_1 t} & \lambda_1 e^{\lambda_1 t} - \lambda_2 e^{\lambda_2 t}\end{bmatrix}\begin{Bmatrix}y_1(0)\\ y_2(0)\end{Bmatrix} \quad (32)$$

4. Time Finite Element Analysis of Chatter Stability

Spatial finite element analysis is used for the estimation of quantities of interest at the nodes of discrete or quantized portions of a continuum. Among other fields of study this type of analysis is used in fluid mechanic to estimate property distribution[10], in vibration analysis to estimate; natural frequencies, mode shapes and forces[11, 12] and in structural analysis to estimate deflections. Ideas from Spatial finite element analysis are utilized for the so-called "time finite element analysis" (TFEA) also called "temporal finite element analysis or finite element in time". TFEA has been variously in used in milling stability investigation[13-15]. Insperger et al[13] wrote that this method was first applied to an interrupted turning process by Halley and Bayly et al. They found that this method only yielded good result when the tool spends most of its cutting period in free flight. This shortcoming was corrected by Bayly et al when they used finer discretization. Stability of regenerative vibration using time finite elements involves dividing the period of cut into E time elements and estimating the perturbation motion of the system in each time element as a linear combination of trial functions. This process allows the formation of a discrete map that forms the substance of stability investigation. Within the present period of cut, the regenerative motion in the $k\,th$ time element becomes

$$z_k(\vartheta) = \sum_i a_{ki}\,\varphi_i(\vartheta) \quad (33)$$

While for the delayed period of cut the motion becomes

$$z_k(\vartheta) = \sum_i a_{ki}^{\tau}\,\varphi_i(\vartheta) \quad (34)$$

The trial functions utilized here are the hermite polynomials[15]

$$\begin{aligned}\varphi_1(\vartheta) &= 1 - 3\frac{\vartheta^2}{{t_k}^2} + 2\frac{\vartheta^3}{{t_k}^3}\\ \varphi_2(\vartheta) &= \left(\frac{\vartheta}{t_k} - 2\frac{\vartheta^2}{{t_k}^2} + \frac{\vartheta^3}{{t_k}^3}\right)t_k\\ \varphi_3(\vartheta) &= \left(3\frac{\vartheta^2}{{t_k}^2} - 2\frac{\vartheta^3}{{t_k}^3}\right)\\ \varphi_4(\vartheta) &= \left(-\frac{\vartheta^2}{{t_k}^2} + \frac{\vartheta^3}{{t_k}^3}\right)t_k\end{aligned} \quad (35)$$

Where ϑ is the local time of the $k\,th$ time element of length t_k. If uniform discretization is carried out then $t_k = \tau/E$. Adopting uniform discretization, substitution of equations (33), (34) and (35) into equation (27) for the $k\,th$ element gives an error of approximation ϵ as

$$\sum_{i=1}^{4}\left\{\ddot{\varphi}_i(\vartheta) + 2\xi\,\omega_n\dot{\varphi}_i(\vartheta) + \left(\omega_n^2 + \frac{wh(\vartheta+(k-1)t_k)}{m}\right)\varphi_i(\vartheta)\right\}a_{ki} - \sum_{i=1}^{4}\left\{\left(\frac{wh(\vartheta+(k-1)t_k)}{m}\right)\varphi_i(\vartheta)\right\}a_{ki}^{\tau} = \epsilon \quad (36)$$

Following the method of weighted residual similar to the Galerki method in spatial finite element analysis, the integral of the weighted error over the $k\,th$ element is set equal to zero giving

$$\begin{aligned}\sum_{i=1}^{4}\int_0^{t_k}\left\{\ddot{\varphi}_i(\vartheta) + 2\xi\,\omega_n\dot{\varphi}_i(\vartheta) + \left(\omega_n^2 + \frac{wh(\vartheta+(k-1)t_k)}{m}\right)\varphi_i(\vartheta)\right\}W_p(\vartheta)d\vartheta\,a_{ki}\\ - \sum_{i=1}^{4}\int_0^{t_k}\left\{\left(\frac{wh(\vartheta+(k-1)t_k)}{m}\right)\varphi_i(\vartheta)\right\}W_p(\vartheta)d\vartheta\,a_{ki}^{\tau} = 0\end{aligned} \quad (37)$$

The weight functions $W_p(\vartheta)$ as utilized in[13] are

$$\begin{aligned}W_1(\vartheta) &= 1\\ W_2(\vartheta) &= \frac{\vartheta}{t_k} - \frac{1}{2}\end{aligned} \quad (38)$$

Customarily nodal quantities are sought for in finite element method thus the nodal perturbations and their derivatives for the $k\,th$ element is seen from equations (33) and (35) taken together to give

$$\begin{aligned} z_k(0) &= a_{k1} \\ \dot{z}_k(0) &= a_{k2} \\ z_k(t_k) &= a_{k3} \\ \dot{z}_k(t_k) &= a_{k4} \end{aligned} \tag{39}$$

The boundary condition that results for two adjacent time elements are

$$\begin{aligned} a_{k1} &= a_{k+1,3} \\ a_{k2} &= a_{k+1,4} \end{aligned} \tag{40}$$

It is already pointed out that free flight could occur for a multi-toothed miller over a time interval $t_f = \frac{30}{\pi\Omega}\left[\frac{2\pi}{N} - (\theta_e - \theta_s)\right]$. Application of equation (32) gives that the state transition matrix $\boldsymbol{\Phi}(t_f) = \frac{1}{\lambda_1-\lambda_2}\begin{bmatrix} \lambda_1 e^{\lambda_2 t_f} - \lambda_2 e^{\lambda_1 t_f} & e^{\lambda_1 t} - e^{\lambda_2 t_f} \\ \lambda_1\lambda_2 e^{\lambda_2 t_f} - \lambda_1\lambda_2 e^{\lambda_1 t_f} & \lambda_1 e^{\lambda_1 t_f} - \lambda_2 e^{\lambda_2 t_f} \end{bmatrix}$ acts as a linear operator over a time interval $t_f = \frac{30}{\pi\Omega}\left[\frac{2\pi}{N} - (\theta_e - \theta_s)\right]$ transforming the end state $\begin{Bmatrix} a_{E3}^{\tau} \\ a_{E4}^{\tau} \end{Bmatrix}$ of last element of delayed period of cut to the start state $\begin{Bmatrix} a_{11} \\ a_{12} \end{Bmatrix}$ of the first element of present period of cut such that

$$\begin{Bmatrix} a_{11} \\ a_{12} \end{Bmatrix} = \begin{bmatrix} \Phi_{11}(t_f) & \Phi_{12}(t_f) \\ \Phi_{21}(t_f) & \Phi_{22}(t_f) \end{bmatrix} \begin{Bmatrix} a_{E3}^{\tau} \\ a_{E4}^{\tau} \end{Bmatrix} \tag{41}$$

Substituting the weight functions $W_p(\vartheta)$, $p = 1$ and 2 independently into equation (37) enables the formation of a local matrix equation for each element which in light of the boundary conditions (40) and (41) are assembled into the global matrix equation of form

$$\mathbf{P}\vec{a} = \mathbf{D}\vec{a}^{\tau} \tag{42}$$

Where both $\mathbf{P}$ and $\mathbf{D}$ are $2(E+1) \times 2(E+1)$ matrices. For example, if three elements are to be used, the global matrix equation becomes

$$\begin{bmatrix} 1 & 0 & 0 & 0 & 0 & 0 & 0 & 0 \\ 0 & 1 & 0 & 0 & 0 & 0 & 0 & 0 \\ P_{11}^1 & P_{21}^1 & P_{31}^1 & P_{41}^1 & 0 & 0 & 0 & 0 \\ P_{12}^1 & P_{22}^1 & P_{32}^1 & P_{42}^1 & 0 & 0 & 0 & 0 \\ 0 & 0 & P_{11}^2 & P_{21}^2 & P_{31}^2 & P_{41}^2 & 0 & 0 \\ 0 & 0 & P_{12}^2 & P_{22}^2 & P_{32}^2 & P_{42}^2 & 0 & 0 \\ 0 & 0 & 0 & 0 & P_{11}^3 & P_{21}^3 & P_{31}^3 & P_{41}^3 \\ 0 & 0 & 0 & 0 & P_{12}^3 & P_{22}^3 & P_{32}^3 & P_{42}^3 \end{bmatrix} \begin{Bmatrix} a_{11} \\ a_{12} \\ a_{21} \\ a_{22} \\ a_{31} \\ a_{32} \\ a_{33} \\ a_{34} \end{Bmatrix} =$$

$$\begin{bmatrix} 0 & 0 & 0 & 0 & 0 & 0 & \Phi_{11}(t_f) & \Phi_{12}(t_f) \\ 0 & 0 & 0 & 0 & 0 & 0 & \Phi_{21}(t_f) & \Phi_{22}(t_f) \\ D_{11}^1 & D_{21}^1 & D_{31}^1 & D_{41}^1 & 0 & 0 & 0 & 0 \\ D_{12}^1 & D_{22}^1 & D_{32}^1 & D_{42}^1 & 0 & 0 & 0 & 0 \\ 0 & 0 & D_{11}^2 & D_{21}^2 & D_{31}^2 & D_{41}^2 & 0 & 0 \\ 0 & 0 & D_{12}^2 & D_{22}^2 & D_{32}^2 & D_{42}^2 & 0 & 0 \\ 0 & 0 & 0 & 0 & D_{11}^3 & D_{21}^3 & D_{31}^3 & D_{41}^3 \\ 0 & 0 & 0 & 0 & D_{12}^3 & D_{22}^3 & D_{32}^3 & D_{42}^3 \end{bmatrix} \begin{Bmatrix} a_{11}^{\tau} \\ a_{12}^{\tau} \\ a_{21}^{\tau} \\ a_{22}^{\tau} \\ a_{31}^{\tau} \\ a_{32}^{\tau} \\ a_{33}^{\tau} \\ a_{34}^{\tau} \end{Bmatrix}$$

where for the $k\,th$ time element

$$P_{ip}^k = \int_0^{t_k} \left\{ \ddot{\varphi}_i(\vartheta) + 2\xi\omega_n \dot{\varphi}_i(\vartheta) + \left(\omega_n^2 + \frac{wh(\vartheta + (k-1)t_k)}{m}\right)\varphi_i(\vartheta) \right\} W_p(\vartheta) d\vartheta \tag{43a}$$

$$D_{ip}^k = \int_0^{t_k} \left\{ \left(\frac{wh(\vartheta + (k-1)t_k)}{m}\right)\varphi_i(\vartheta) \right\} W_p(\vartheta) d\vartheta \tag{43b}$$

As long as $\mathbf{P}$ is non-singular, the global matrix equation can be put in the form

$$\vec{a} = \mathbf{P}^{-1}\mathbf{D}\vec{a}^{\tau} = \mathbf{M}\vec{a}^{\tau} \tag{44}$$

Equation (44) is a $2(E+1)$-dimensional discrete time map of the system. It is seen that the nodal state vectors combine to form the global state vector of the discrete map. The matrix $\mathbf{M}$ acts as a linear operator that transforms the delayed state $\vec{a}^{\tau}$ to the present state $\vec{a}$. The matrix $\mathbf{M}$ is called the monodromy matrix of the system. The nature of its eigenvalues also called characteristic multipliers determines the condition of stability of the system. The necessary and sufficient condition for asymptotic stability of the system is that each of the eigenvalues of the monodromy matrix has a magnitude that is less than one. In other words, all the eigen-values of the matrix $\mathbf{M}$ must exist within a unit circle centred at the origin of the complex plane. Since the magnitude of the eigen-values depends on the cutting parameter combination, the parameter space of the system has to be demarcated into stable and unstable domains. This is achieved on the cutting parameter plane of spindle speed and depth of cut by tracking the stability transition curve along which the maximum magnitude characteristic multiplier lies on the unit circle. The two types of loss of stability (bifurcation) that are analytically and experimentally established for milling are[4]

i. Period two or period doubling or flip bifurcation in which the exit of the unit circle of the critical characteristic multiplier μ is at -1.

ii. Secondary Hopf or Neimark-Sacker bifurcation which involves a pair of complex conjugate characteristic multiplier leaving the unit circle.

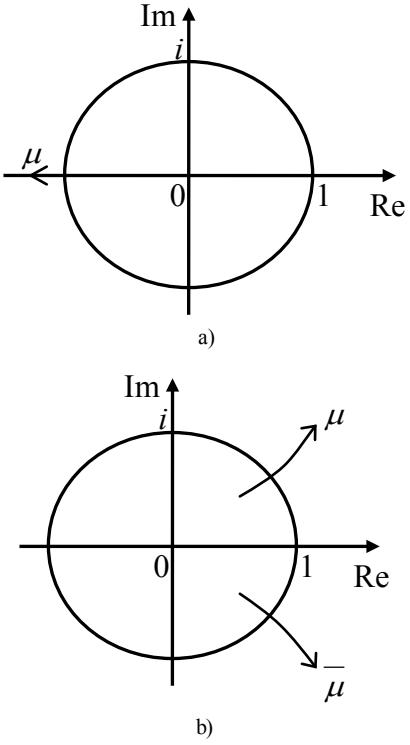

Figure 9. (A) Flip Bifurcation (B) Secondary Hopf Bifurcation

5. Results and Validation

Making use of the relevant equations enables the eigen-value analysis of the monodromy matrix of reference system with specification; $m = 0.0431$ kg, $\omega_n = 5700$ rad/sec, $\xi = 0.02$, $C = 3.5 \times 10^7\,\mathrm{Nm}^{-7/4}$ and $v = 0.0025$ m/s on the parameter plane of spindle speed Ω and depth of cut w leading to the stability charts of figures 10, 11 and 12 for 0.5, 0.75 and 0.8 radial immersions respectively. MATLAB contour command is utilized in the eigen-value analysis. Each of the stability charts is generated using 14 elements causing computation time per chart of a computer with processing speed of 2.10 Ghz to be about 2.92 hrs. The stable sub domain of each stability chart is left white while the unstable sub domain is filled dark.

Though machine tools have a random pre-function (or history), stability information of a cutting parameter combination can still be fixed by assuming a constant pre-function since it is found that magnitude of such a pre-function has no effect on stability in large[5]. Making use of any constant history, equation (28) is solved using MATLAB dde23 at some chosen points of the stability charts. Stable MATLAB dde23 solutions exhibit decaying perturbation with time and are marked with star while the unstable ones exhibit growing perturbation with time and marked oval on the charts. Close agreement between the charts and MATLAB dde23 solutions attests to validity of the charts. For illustration some of the MATLAB dde23 solutions are presented in the form of phase trajectories as shown in figure 13. It is seen that stable trajectories (a, b and f of figure 13) collapse to zero motion with time evolution while the unstable ones (b, d and e of figure 13) diverge from initial condition $\{y_1(0) \quad y_2(0)\}^T = \{0.0000001 \quad 0.000001\}^T$.

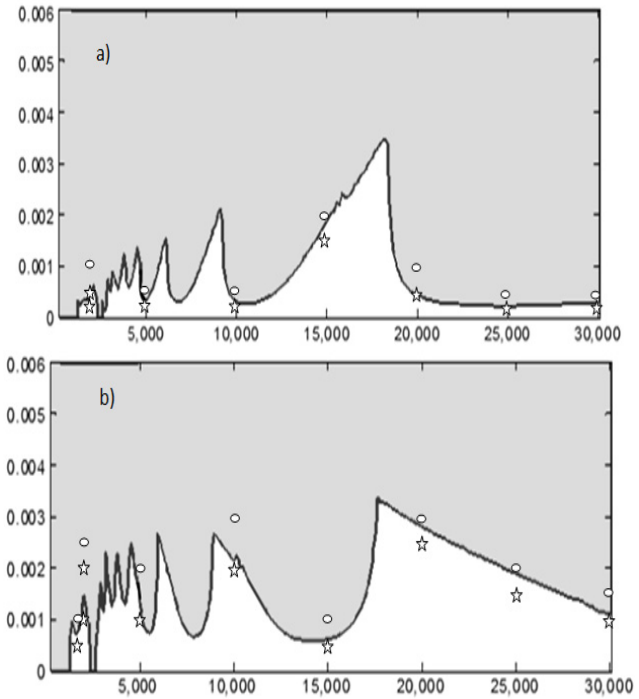

Figure 10. Stability Charts At ρ =0.5 with Stable Sub Domain Left White and the Unstable Sub Domain Filled Dark (A) Up End-Milling (B) Down End-Milling

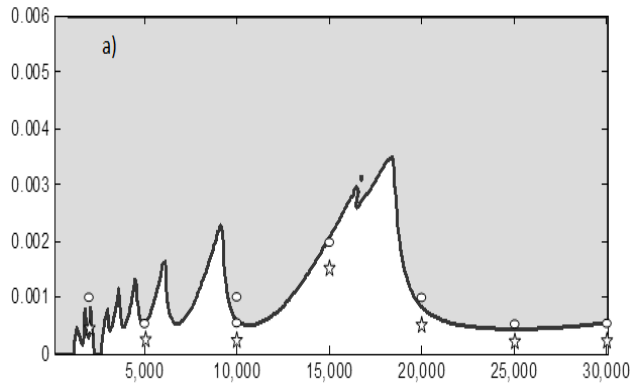

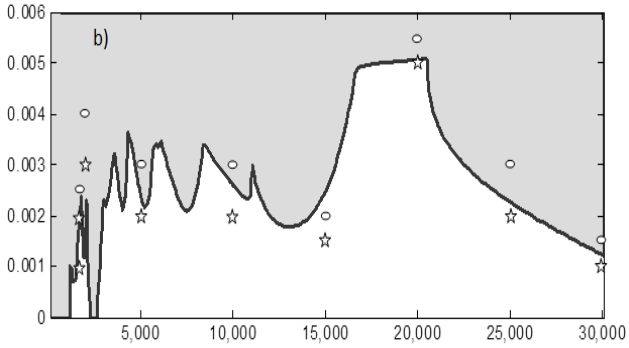

Figure 11. Stability Charts At ρ =0.75 with Stable Sub Domain Left White and the Unstable Sub Domain Filled Dark (A) Up End-Milling (B) Down End-Milling

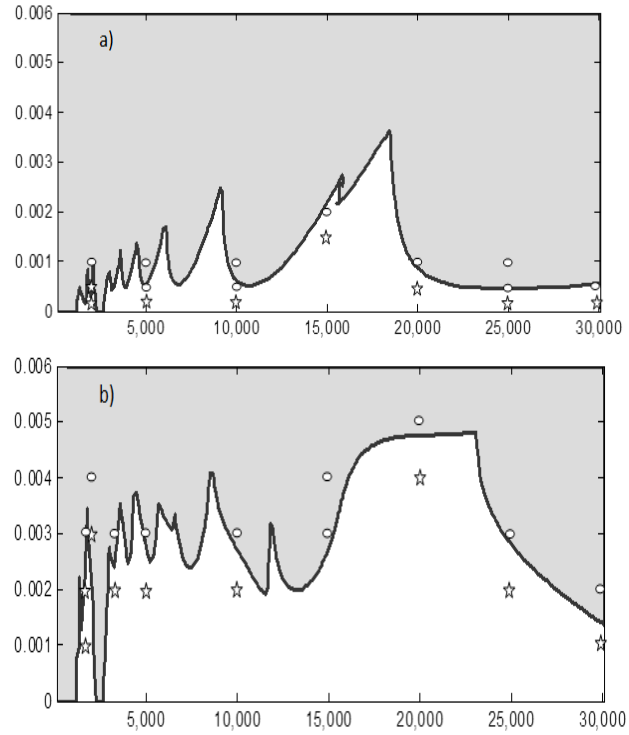

Figure 12. Stability Charts at ρ =0.8 with Stable Sub Domain Left White and the unstable sub domain filled dark (a) up end-milling (b) down end-milling

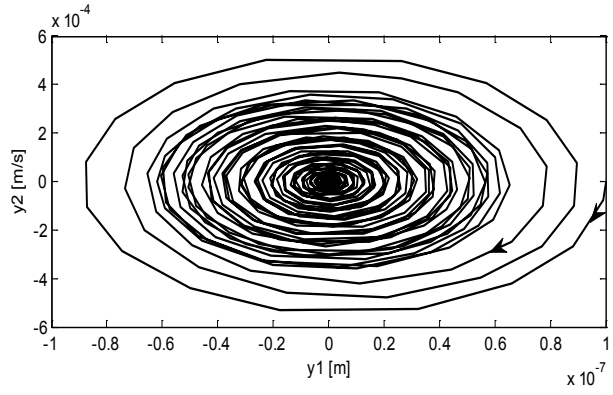

a)

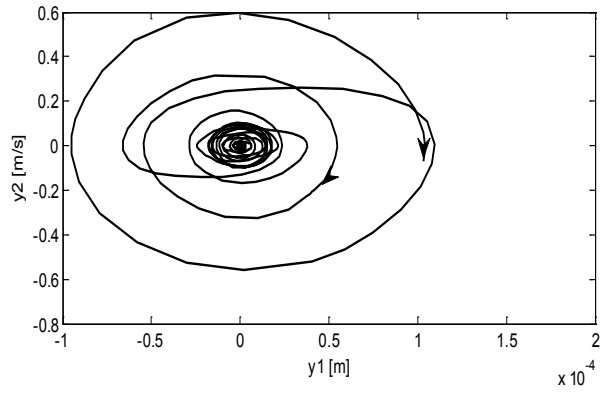

b)

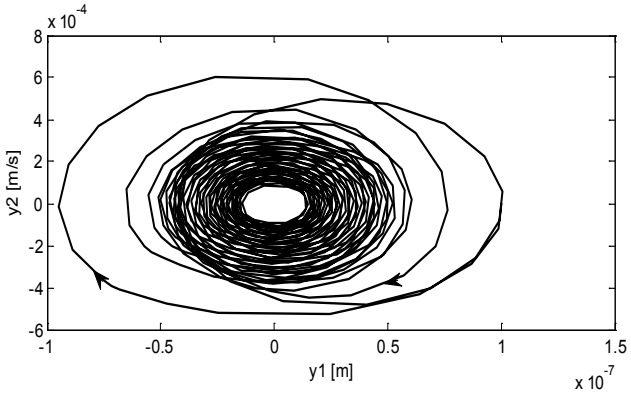

c)

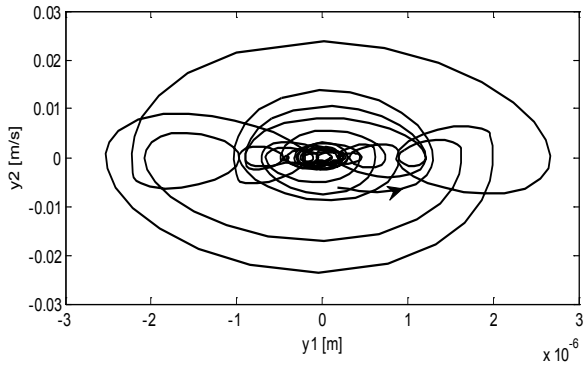

d)

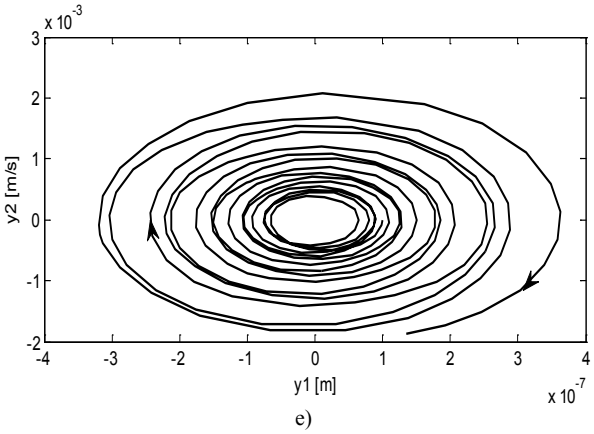

e)

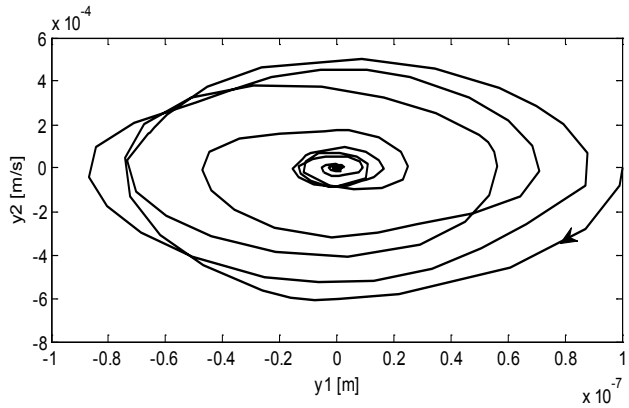

f)

Figure 13. SAMPLE PHASE TRAJECTORIES (a) UP END-MILLING AT $\boldsymbol{\rho}$ =0.5, $\boldsymbol{w}$=0.25 mm AND Ω =5000 rpm (b) $\boldsymbol{\rho}$ =0.5, $\boldsymbol{w}$ =3 mm AND Ω =10000 rpm (c) $\boldsymbol{\rho}$ =0.75, $\boldsymbol{w}$ =1.5 mm AND Ω =15000 rpm (d) $\boldsymbol{\rho}$ =0.75, $\boldsymbol{w}$ =5.5 mm AND Ω =20000 rpm (e) $\boldsymbol{\rho}$ =0.8, $\boldsymbol{w}$ =0.5 mm AND Ω =25000 rpm (f) $\boldsymbol{\rho}$ =0.8, $\boldsymbol{w}$ =1 mm AND Ω =30000 rpm

6. Discussions

It is seen that the down end-milling mode is more stable than the up end-milling mode. To quantify the superiority of chatter stability of down end-milling over up end-milling, numerical integration means such as trapezoidal or Simpson's rule is utilized to approximate the area under each stability transition curve. The Simpson's rule[16, 17] to estimate the area of stable subspace of each of the stability charts is

$$A = \frac{\Delta\Omega}{3}\left(w_o + w_n + \sum_{i\ odd} 4w_i + \sum_{i(\neq n)even} 2w_i\right) \quad (45)$$

Where $\Delta\Omega = (\Omega_n - \Omega_0)/n$ is the steps of spindle speed, n is an even number into which the stable area is divided and $i = 0, 1, 2, \ldots\ldots\ldots n$ are the mesh points. $w_i = w(\Omega_i)$ and $\Omega_i = i\Delta\Omega$. Making use of $\Omega_0 = 100$, $\Omega_n = 30000$ and $n = 60$ in equation (45), an estimation of stable area of the charts is as summarized in table1.

It is seen from table1 that for the radial immersions considered, up end-milling operations are much less stable than the down end-milling operations. Switching from up end-milling mode to down end-milling mode at 0.5 radial immersion almost doubles the possibility of chatter free milling in the spindle speed range $0 < \Omega \leq 30000$ while at 0.75 and 0.8 radial immersions, this possibility almost triples in the same spindle speed range. Since productivity is measured in terms of material removal rate, it is proportional to the product of depth of cut and radial immersion. This means that the down end-milling mode allows freer choice of very productive stable operation. It is already established that up end-milling operation is more damaging to tool than down end-milling operation since it generally has higher periodic cutting force amplitude over the whole radial immersion range. Thus it is strongly recommend that an end-milling operation at partial radial immersion is carried out in the down end-milling mode for better product quality and longevity of tool and machine structure.

Table 1. Area of Stable Domain of the Stability Charts of Figures 10, 11 and 12

Radial immersion	Stable area of up end-milling[m rpm]	Stable area of down end-milling[m rpm]	Percentage rise in stable area[m rpm]
0.5	22.9	43.4	89.52
0.75	29.55	78.75	166.5
0.8	30.65	85.85	180.1

7. Conclusions

End-milling at partial radial immersion is seen to have two distinct modes. One of the modes which dynamically looks like the conventional milling is called "up end-milling" while the other that dynamically resembles the climb milling is called "down end-milling". It results from analysis of cutting force and chatter stability that the down end-milling mode is better favoured for workshop application than the up end-milling mode. This is because up-end-milling is considered to be more damaging to tool than the down end-milling since it generally has higher periodic cutting force amplitude. The superiority of chatter stability of down end-milling over up end-milling is quantified by making use of the Simpson's rule to establish that switching from up end-milling mode to down end-milling mode at 0.5 radial immersion almost doubles the possibility of chatter free milling in the spindle speed range $0 < \Omega \leq 30000$ while at 0.75 and 0.8 radial immersions this possibility almost triples in the same spindle speed range. This result is in conformity with the age long recognition from workshop practices that climb milling operations are more stable than conventional milling operations. Validation of the resulting stability charts is conducted using MATLAB dde23 analysis of selected points on the parameter plane of spindle speed and depth of cut.

REFERENCES

[1] Youssef, H. A. and El-Hofy, H., 2008, *Machining Technology: Machine Tools and Operations,* CRC Press Taylor &Francis Group, pp.

[2] Joshi, P. H., 2007, *Machine Tools Handbook: Design and Operation,* Tata McGraw-Hill Publishing Company Limited, New Delhi, pp.40-41.

[3] Miller, R. and Miller, M. R., *Machine Shop Tools and Operations*, All new 5th edi., Willey Publishing Inc., New York, pp.253-254.

[4] Insperger, T., *2002,* "Stability Analysis of Periodic Delay-Differential Equations Modelling Machine Tool Chatter," PhD thesis, Budapest University of Technology and Economics.

[5] Ozoegwu, C. G., *2011,* "Chatter of Plastic Milling CNC Machine," M. Eng thesis, Nnamdi Azikiwe University Awka.

[6] Gatti, P. L., and Ferrari, V., 2003, *Applied Structural and Mechanical Vibrations: Theory, methods and measuring instrumentation*, Taylor & Francis e-Library.

[7] He, J. and *Fu, Z., 2001, Modal Analysis*, Butterworth Heinemann, Oxford.

[8] Rao, S. S., 2004, *Mechanical Vibrations* (4th ed.), Dorling Kindersley, India.

[9] Stepan, G., 1998, Delay-differential Equation Models for Machine Tool Chatter: in Nonlinear Dynamics of Material Processing and Manufacturing, edited by F. C. Moon, John Wiley & Sons, New York, p. 165-192.

[10] Ihueze, C. C. and Ofochebe, S. M., 2011, "Finite Design for Hydrodynamic Pressure on Immersed Moving Surfaces," International Journal of Mechanics and Solids, 6(2), pp.115-128.

[11] Ihueze, C. C., Onyechi, P. C., Aginam, H. and Ozoegwu, C. G., 2011, "Finite Design against Buckling of Structures under Continuous Harmonic Excitation," International Journal of Applied Engineering Research, 6(12), pp.1445-1460.

[12] Ihueze, C. C., Onyechi, P. C., Aginam, H. and Ozoegwu, C. G., 2011, "Design against Dynamic Failure of Structures with Beams and Columns under Excitation," International Journal of Theoretical and Applied Mechanics, 6(2), pp.153-164

[13] Insperger, T., Mann, B.P., Stepan, G., and Bayly, P. V., 2003, "Stability of up-milling and down-milling, part 1: alternative analytical methods," International Journal of Machine Tools & Manufacture, 43, pp.25–34.

[14] Bobrenkov, O. A., Khasawneh, F. A., Butcher, E. A. and Mann, B. P., 2010, "Analysis of milling dynamics for simultaneously engaged cutting teeth," Journal of Sound and Vibration, 329, pp.585–606.

[15] Bayly, P.V., Schmitz, T. L., Stepan, G., Mann, B. P., Peters, D. A. and Insperger, T., 2002, "Effects of radial immersion and cutting direction on chatter instability in end-milling," Proceedings of IMECE'02 2002 ASME International Mechanical Engineering Conference & Exhibition New Orleans, Louisiana, November 17-22.

[16] Riley, K. F., Hobson, M. P. and Bence, S. J., 1999, *Mathematical Methods for Physics and Engineering*, Low Prize ed., Cambridge University Press, pp.185.

[17] Jain, M. K., Iyengar, S. R. K. and Jain, R. K., 2007, *Numerical Methods for Scientific and Engineering Computation*, Fifth ed., New Age International (P) Limited Publishers, pp.352 and 357.